DOI 10.1007/s11182-021-02249-x
Russian Physics Journal, Vol. 63, No. 11, March, 2021 (Russian Original No. 11, November, 2020)

DEFORMATION EFFECT ON MICROTWINNING AND CRYSTAL LATTICE DISTORTION OF POLYCRYSTALLINE Cu–Al ALLOYS

N. A. Koneva,[1] L. I. Trishkina,[1] T. V. Cherkasova,[1,2] A. N. Solov'ev,[1] and N. V. Cherkasov[1]

UDC 669.35:539.214

The paper considers the dynamics of changing of misoriented dislocation substructures appearing at a stage of developed plastic deformation. The types of defects, which induce the distortion of the crystal lattice are studied in detail. The quantitative parameters are obtained for the lattice distortion in alloys at a different grain size. It is found that the lattice bending and torsion parameters in the misoriented cellular-network and microtwin substructures depend on the degree of deformation. The lattice distortion is investigated both in the vicinity and far from the microtwins. It is shown that the microtwin formation occurs with increasing deformation at a different grain size.

Keywords: metals, alloys, deformation, grain size, bending-torsion amplitude of crystal lattice, microtwinning.

INTRODUCTION

Deformation of metallic materials induces different defects in their crystal lattices. One of the most important defects is the lattice bending [1–4]. Localized bending of the crystal lattice is provided by the material deformation, it determines the nucleation of dislocations, contributes to the strain hardening, promotes the crack formation and, finally, leads to the material fracture [5]. Let us determine the lattice bending as its distortion. According to [4, 6], the localized bending develops along with the material deformation at all the scale levels, determines the nucleation of dislocations, contributes to the strain hardening, promotes the crack formation and, leads finally to the material fracture. Generally, the lattice distortion is a tensor consisting of the bending and torsion components. The lattice bending and torsion in the face-centered cubic (FCC) crystal systems of polycrystalline solid solution originate from the grain boundaries and kinks, grain-boundary intersections, excess dislocations in the bulk material, disclinations and microcracks [7, 8]. The transmission electron microscopy (TEM) observations of deformed materials show that the lattice bending and torsion represent bend extinction contours. There is very little information offered in the literature concerning the experimental studies of the evolution of the lattice distortion and its dependence on the grain size.

The aim of this work is to determine the influence of the grain size and the density of dislocations in different types of dislocation substructures, such as misoriented cellular-network and microtwin substructures, on the deformation-induced lattice distortion. It is shown that the relation between the lattice distortion and the dislocation density in the misoriented cellular-network substructure depends on the distance to the microtwins.

[1]Tomsk State University of Architecture and Building, Tomsk, Russia, e-mail: koneva@tsuab.ru; trishkina.53@mail.ru; cherkasova_tv@mail.ru; tsk_san@mail.ru; cherkasov_2000@outlook.com; [2]National Research Tomsk Polytechnic University, Tomsk, Russia. Translated from Izvestiya Vysshikh Uchebnykh Zavedenii, Fizika, No. 11, pp. 63–67, November, 2020. Original article submitted July 31, 2020.

MATERIALS AND METHODS

Polycrystalline FCC alloys Cu–10 at.% Al and Cu–14 at.% Al were used in this experiment. The test machine INSTRON was used to measure tensile strength of 100×12×2 mm specimens at 293 K and $2 \cdot 10^{-2}$ s^{-1} strain rate. Observations of the structure of thin foils were made on the EMV-100 AK transmission electron microscope and Tesla BS-540 transmission electron microscope equipped with goniometer providing tilt and precision rotation. The grain size of the alloy specimens ranged from 10 to 200 μm. The parameters of the lattice bending and torsion as well as the microtwin density were determined by using the TEM images.

The lattice distortion χ is calculated from the gradient of continuous misorientation [9, 10]:

$$\chi = \frac{\partial \varphi}{\partial \ell},$$

where φ is the tilt angle of the crystallographic plane relative to the electron beam, ℓ is the distance on the crystallographic plane. The value of $d\varphi/d\ell$ is obtained by using the parameters of bend extinction contours. The latter are localized in the region with the similar orientation of reflecting planes. The χ value can be derived from measurements of the width $\Delta\ell$ of the bend extinction contour in the localized regions, at a constant tilt angle of the specimen. The density of microtwins was detected on micrographs using the secant method [11]. The detailed description of the methods utilized is given in [12].

RESULTS AND DISCUSSION

In polycrystalline alloys high in an allying element, the formation of the microtwin substructure begins at $\varepsilon_{true} > 0.10$ deformation associated with the misoriented cellular-network substructure. TEM images in Fig. 1 demonstrate the microtwin substructure at different deformation degrees. In Fig. 1*a*, one can see the formation of single microtwins at $\varepsilon_{true} = 0.10$. According to Fig. 1*b*, a packet of microtwins appears with increasing deformation up to $\varepsilon_{true} = 0.30$, and then the formation of two (Fig. 1*c*) or more (Fig. 1*d*) microtwin packets occurs. Microtwins in alloys can appear both inside the grain (Fig. 1*a*–*c*) and from the grain boundaries, as presented in Fig. 1*d*. These microtwins induce bending and torsion of the crystal lattice. This is proven by the bend extinction contours forming from microtwins.

Figure 2 contains the plots of microtwin density/strain relations for the different grain size. According to these plots, with increasing deformation, the intensive formation of microtwins occurs from several slip systems and the microtwin density grows at any grain size. With increasing grain size, the microtwin density also grows, whereas the average scalar dislocation density lowers in the misorineted cellular-network substructure. It should be noted that the increase in the microtwin density leads to a decrease in the dislocation density. This shows that microtwinning hinders the slip process in the material.

In Fig. 3, the dependences describe the dislocation density of the misorineted cellular-network substructure and the distance to the microtwins. In the vicinity of the microtwins we observe the low dislocation density at a grain size of 10 and 200 μm. The growth in the dislocation density occurs with increasing distance from the microtwins, and then becomes constant.

At a higher deformation degree, the bend extinction contours intensively develop, that indicates the structural misorinetations, which lead to the lattice distortion. Figure 4 presents a plot of the lattice distortion/deformation degree dependence for 10 and 200 μm grain size an average of the specimen, i.e., with regard to the lattice distortion in the misorineted cellular-network and microtwin substructures. According to this plot, the lattice distortion increases with increasing deformation.

The dependences between the lattice distortion χ and the distance X from the microtwins at different deformation degrees are plotted in Fig. 5 for two grain sizes. The lattice distortion χ lowers with increasing distance X from the microtwins. Let us discuss the microtwin behavior during the lattice bending and torsion depending on the formation of the bend extinction contour with increasing distance X. Firstly, the width of the extinction contour does not

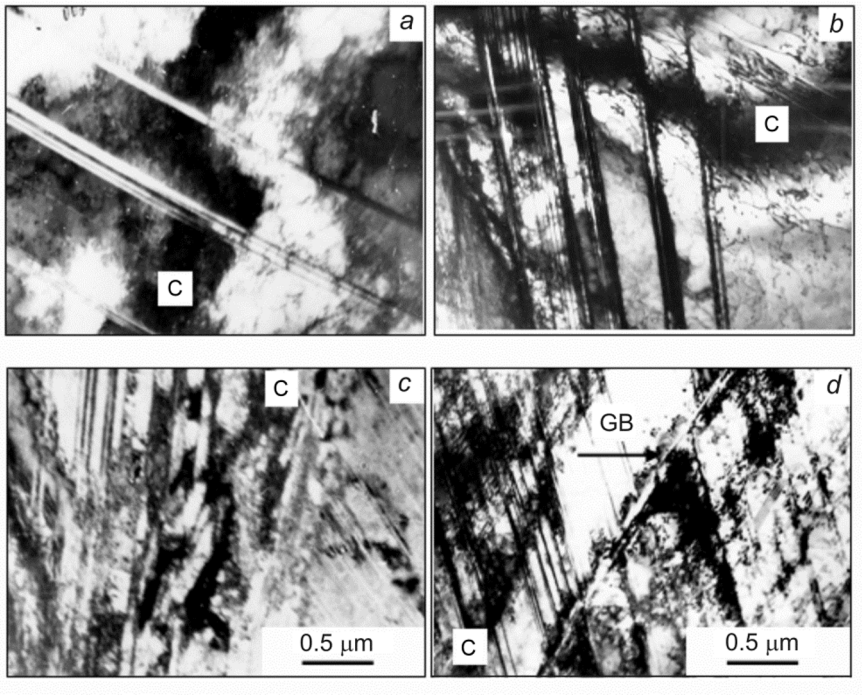

Fig. 1. TEM images of microtwins in Cu–10 at.% Al alloy at different deformations: *a* – single microtwins ($\varepsilon_{true} = 0.10$), *b* – one microtwin packet ($\varepsilon_{true} = 0.30$), *c* – two microtwin packets ($\varepsilon_{true} = 0.40$), *d* – microtwin formation from the grain boundaries ($\varepsilon_{true} = 0.50$). K and GB denote the extinction contour and the grain boundary, respectively.

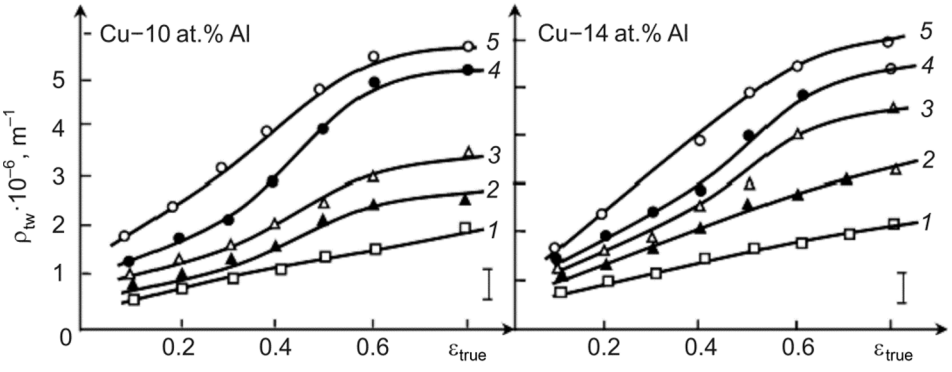

Fig. 2. Microtwin density/strain relations for different grain sizes: *1* – 10 μm, *2* – 40 μm, *3* – 60 μm, *4* – 120 μm, *5* – 240 μm.

change; secondly, it grows; and thirdly, reduces. This is shown in Fig. 6, where in the first case the lattice distortion χ does not change (curve *1*), in the second case it lowers (curve *2*), and in the third case it grows (curve *3*).

The lattice distortion χ does not change, if the extinction contour appears between two mocrotwins, i.e., when microtwins form a packet. The lattice distortion χ is linearly dependent of the microtwin density, as shown in Fig. 7.

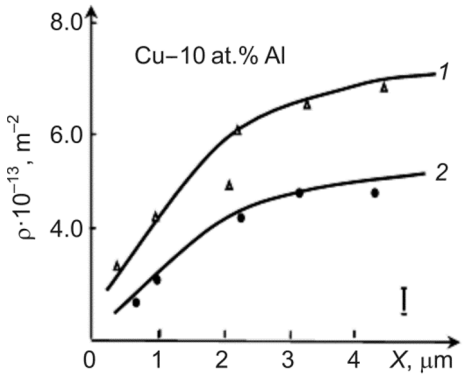

Fig. 3

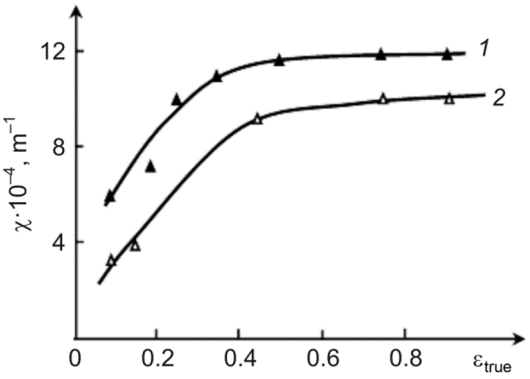

Fig. 4

Fig. 3. Dependences between the dislocation density of misorineted cellular-network substructure and the distance *X* to the microtwins at different grain sizes: *1* – 10 μm, *2* – 200 μm.

Fig. 4. Lattice distortion/deformation degree dependence in Cu–10 at.% Al alloy at different grain sizes: *1* – 10 μm, *2* – 200 μm.

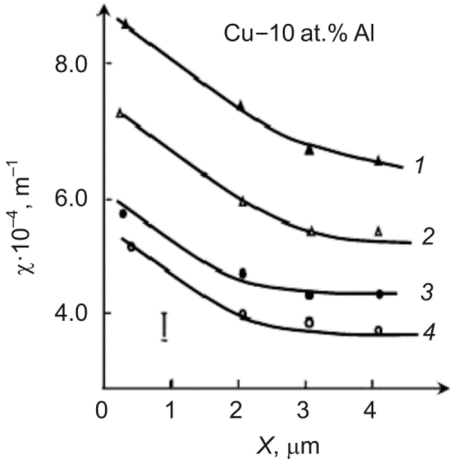

Fig. 5

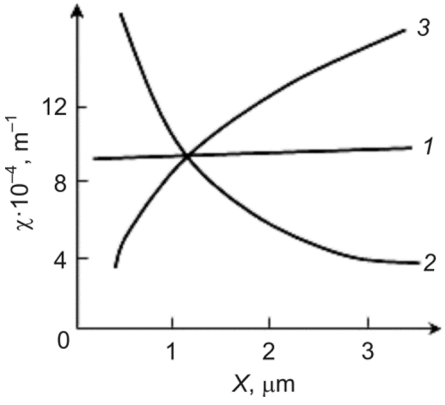

Fig. 6

Fig. 5. Lattice distortion/distance *X* dependence at different degrees of deformation: *1*, *2* – ε_{true} = 0.40, *3*, *4* – ε_{true} = 0.10. Grain size: *1*, *3* – 10 μm, *2*, *4* – 200 μm.

Fig. 6. Schematic dependence between lattice distortion χ and distance *X* from microtwins with regard to the width of bend extinction contours (curves *1–3*).

CONCLUSIONS

TEM investigations of the misoriented cellular-network and microtwin substructures were carried out at different deformation degrees and grain sizes. The lattice bending and torsion were studied in deformed Cu–Al

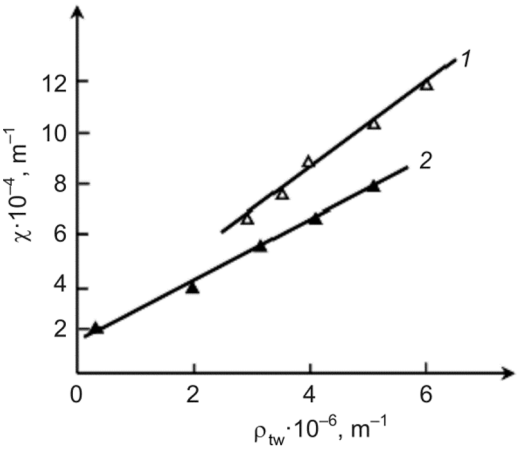

Fig. 7. Lattice distortion/ microtwin density ρ_{tw} in alloys: *1* – Cu–10 at.% Al, *2* – Cu–14 at.% Al.

polycrystalline alloys. It was found that the lattice bending and torsion were induced by the misoriented cellular-network and microtwin substructures and linearly depended on the microtwin density. The maximum dislocation density was observed on a large distance from the microtwins.

This work was carried out within the government contract N FEMN-2020-0004 of the Ministry of Science and Higher Education of the Russian Federation

REFERENCES

1. N. A. Koneva, L. I. Trishkina, D. V. Lychagin, and E. V. Kozlov, New Methods in Physics and Deformable Body Mechanics. Part 1 [in Russian], V. E. Panin, ed., TSU, Tomsk (1990), pp. 83–93.
2. A. N. Tyumentsev, I. A. Ditenberg, A. D. Korotaev, and K. I. Denisov, Fizich. mezomekh., **16**, No. 3, 63–79 (2013).
3. A. N. Tyumentsev, A. D. Korotaev, and Yu. P. Pinzhin, Fizich. mezomekh., **7**, No. 4, 35–53 (2004).
4. V. E. Panin, A. V. Panin, T. F. Elsukova, and Yu. F. Popkova, Fizich. mezomekh., **17**, No. 6, 7–18 (2014).
5. N. A. Koneva, L. I. Trishkina, T. V. Cherkasova, and E. V. Kozlov, Bull. Russ. Acad. Sci. Phys., **81**, No. 3, 391–393 (2017).
6. V. E. Panin and V. E. Egorushkin, Fizich. mezomekh., **18**, No. 3, 100–113 (2015).
7. N. A. Koneva, L. I. Trishkina, and E. V. Kozlov, Bull. Acad. Sci. USSR, Phys. Ser., **62**, No. 7, 391–393 (1998).
8. N. A. Koneva, L. I. Trishkina, T. V. Cherkasova, Russ. Phys. J., **60**, No. 4, 570–576 (2017).
9. E. V. Kozlov, D. V. Lychagin, N. A. Koneva, *et. al*., Physics of Strength of Heterogeneous Materials [in Russian], A. E. Romanov, ed., Ioffe Institute, Leningrad (1988), pp. 3–13.
10. N. A. Koneva, L. I. Trishkina, and T. V. Cherkasova, Bull. Russ. Acad. Sci. Phys., **83**, No. 10, 1362–1367 (2019).
11. S. A. Saltykov, Stereometric Metallography [in Russian], Metallurgiya, Moscow (1970).
12. N. A. Koneva, T. V. Cherkasova, L. I. Trishkina, *et al*., Dislocation Structure and Dislocation Substructures. Electron Microscopy for Parameter Measurements [in Russian], SibGIU, Novokuznetsk (2019).